

SUPPORTING INFORMATION

for

Unusually high energy barriers for internal conversion in a {Ru(bpy)} chromophore

Agustina Cotic,^{a,b} Koen Veys,^c Daniel Escudero,^{c,*} Alejandro Cadrenal^{a,b,d,e,*}

^a Universidad de Buenos Aires, Facultad de Ciencias Exactas y Naturales, Departamento de Química Inorgánica, Analítica y Química Física, Pabellón 2, Ciudad Universitaria, C1428EHA, Buenos Aires, Argentina.

^b CONICET – Universidad de Buenos Aires, Instituto de Química-Física de Materiales, Medio Ambiente y Energía (INQUIMAE), Pabellón 2, Ciudad Universitaria, C1428EHA, Buenos Aires, Argentina.

^c Department of Chemistry, KU Leuven, 3001 Leuven, Belgium

^d Friedrich-Alexander-Universität Erlangen-Nürnberg (FAU), Physical Chemistry I, Egerlandstr. 3, 91058, Erlangen, Germany.

^e Friedrich-Alexander-Universität Erlangen-Nürnberg (FAU), Interdisciplinary Center for Molecular Materials, Egerlandstr. 3, 91058, Erlangen, Germany.

Table of Contents

Experimental Details	3	Table S3	14
Computational Details	3	Table S4	15
FCLA	5	Table S5	16
Figure S1	5	Table S6	17
nsTAS and fsTAS measurements at different temperatures	6	Table S7	18
Figure S2	6	Contributions to the observed decay constants for LE-³MLCT and HE-³MLCT	19
Figure S3	7	Figure S8	19
Table S1	8	Figure S9	19
Observations	9	Density descriptors for excited state interconversions	20
Figure S4	10	Figure S10	20
Theoretical Calculations	11	Solvent dependence of IC rates	21
Figure S5	11	Figure S11	21
Figure S6	12	References	22
Table S2	13		
Figure S7	13		

Experimental Details

RuNCS was available from a previous study.^[1]

Steady-state emission spectroscopy was performed on a Horiba Jobin Yvon Fluoromax 3 using argon-saturated solutions in 1 cm optical path cuvettes. An Optistat DN cryostat from Oxfrod Instruments was employed for temperatures between room temperature and 80 K. Photoluminescence quantum yields were obtained by comparative actinometry using $[\text{Ru}(\text{bpy})_3]^{2+}$ as a reference.^[2]

Ultrafast transient absorption experiments were conducted using an amplified Ti:sapphire fs laser system (Clark MXR CPA2101 and CPA2110, 1kHz, FWHM = 150 fs, $\lambda^{\text{exc}} = 500$ nm, 300-700 nJ per pulse) with TA pump / probe Helios (fsTAS) or EOS (nsTAS) detection system from Ultrafast Systems. In fsTAS experiments, white light was generated focusing a fraction of the fundamental 775 nm output onto a 2 mm sapphire disk (~ 430 –760 nm). In nsTAS experiments, white light (~ 370 to >1600 nm) was generated by a built-in photonic crystal fiber supercontinuum laser source with a fundamental of 1064 nm at 2 kHz output frequency and pulse width of approximately 1 ns. A magic angle configuration between the pump and the probe beams was employed to avoid rotational dynamics. Excitation pulses were generated by a NOPA. Bandpass filters with ± 5 or ± 10 nm were used to ensure low spectral width and to exclude 775 nm photons. Typical excitation spot areas are around 500 nm and ensured to be larger than those of the probe beam. All measurements were conducted in a 2 mm quartz cuvette under argon atmosphere, using solutions with room temperature absorbances of 0.5-0.7. Sample holders were coupled to a Peltier thermoelectric device for temperatures above room temperature, or to an Optistat DN cryostat from Oxfrod Instruments for temperatures between room temperature and 80 K.

To analyze transient absorption data, we used a suggested procedure.^[3] We start with SVD and global analysis, using an all-sequential decay model that provides evolution associated spectra of potentially intervening species, to determine the number of decaying species that participate in the decay cascade. However, this doesn't necessary yield differential spectra with genuine physicochemical meaning. Afterwards, a target analysis is applied, using specific target models that result in species associated spectra with true physicochemical meaning. Obtained data were treated by SVD, global and target analyses using the R- package TIMP and GloTarAn.^{[3]-[5]}

Fittings of temperature dependent PLQY, nsTAS and fsTAS were performed using OriginLab software. Fitting of nsTAS and fsTAS data required to fix $(k_{\text{dr}} + k_{\text{dnr}})$. As an approximation, we employed the limit values of 8.81×10^5 and $1.08 \times 10^7 \text{ s}^{-1}$, respectively, observed at 80K and 120 K, respectively, where contributions from activated terms is minor. For fsTAS, where the approximation with the value at 120 K could be an overestimation, we verified that using fixed values between 1×10^4 - 1×10^8 did not significantly affect the resulting AIC and E_{AIC} outcomes.

FCLA was performed using a reported software.^[6]

Computational Details

Geometry optimizations and frequency calculations of the singlet ground state and first three excited triplet states were performed with respectively density functional theory (DFT)^{[7]-[10]}

and Time-Dependent DFT (TD-DFT)^{[11],[12]} with the B3LYP^[13] functional. For all atoms except Ru, the 6-31G(d)^[14] basis set was used, while the MWB28^[15] effective core potential (ECP) and basis set were used for Ru. The effect of solvent (propionitrile) was included using the integral equation formalism polarizable continuum model (IEF-PCM).^[16]

For the simulation of the ESA spectra, single point TDDFT calculations were performed on the T₁₋₃ optimized geometries including up to 50 triplet states, using the same level of theory as in the optimizations. All these calculations were carried out with the Gaussian 16A03 package,^[17] using the default parameters. The transition oscillator strengths in the latter calculations (f_{trans}) were calculated from the gaussian outputs using the Multiwfn-3.7 program.^{[18],[19]} Afterwards, the line spectra (f_{trans} vs ΔE_{if}) were convoluted with a gaussian broadening function to match the experimental broadening. Ground state bleach (GSB) was calculated similarly, using the first 5 singlet state energies and oscillator strengths (f) at the ground state geometry and convoluting this with the same broadening function.

Phosphorescence spectra were obtained with the ESD module,^[20] as implemented in Orca 5.0.3. Towards this end, the frequencies were firstly recalculated on top of the previously optimized TD-B3LYP geometries, using TD-DFT with the orca implementation of B3LYP and the zeroth order regular approximation (ZORA)^[21] Hamiltonian to account for relativistic effects. The all-electron ZORA-Def2-TZVP^[22] basis set (and the adapted SARC-ZORA-TZVP for Ru) was used together with the spin-orbit mean field operator (SOMF) to include the spin-orbit coupling. Inclusion of solvent was done by the conductor-like polarizable continuum model (CPCM)^[23] scheme, using propionitrile as solvent. Furthermore, SCF-convergence was set to tight, and the RI approximation^[24] was invoked to accelerate the evaluation of the integrals. Next, the ESD calculations were carried out using the adiabatic hessian model in cartesian coordinates and with a temperature of 298K. Duschinsky rotation effects were included, but Herzberg-Teller effects were not. The rate and spectra were calculated for all three ($M_s = -1, 0, +1$) spin-sublevels of the triplet state and were added to get the final rate.

The optimization of the minimum energy conical intersection (MECI) between T₂ and T₃ was performed with spin-flip (SF)-TD-DFT,^[25] as implemented in the QChem 5.3 package.^[26] The latter calculations were performed using the B3LYP functional and the LANL2DZ basis sets and effective core potentials. Solvent effects were included with the conductor-like polarizable continuum model (CPCM) scheme, using propionitrile as solvent. Single point TD-DFT calculations were performed with the 6-31G(d) basis set and the MWB28 effective core potential (ECP) for Ru to estimate the internal conversion barrier with a coherent computational protocol. Note that while at the SF-TD-DFT level T₂ and T₃ are, as expected, degenerate (<0.02 eV energy difference), the degeneracy is slightly lifted at the TD-DFT level of theory (ca. 0.1 eV energy difference). This leads to a lower-bound estimation of the barrier of 1043 cm⁻¹ (based on the T₂ energy) and an upper-bound estimation of the barrier of 2216 cm⁻¹ (based on the T₃ energy).

The XYZ coordinates of the optimized S₀, T₁₋₃ and MECI geometries are collected in Tables S3-S7.

FCLA

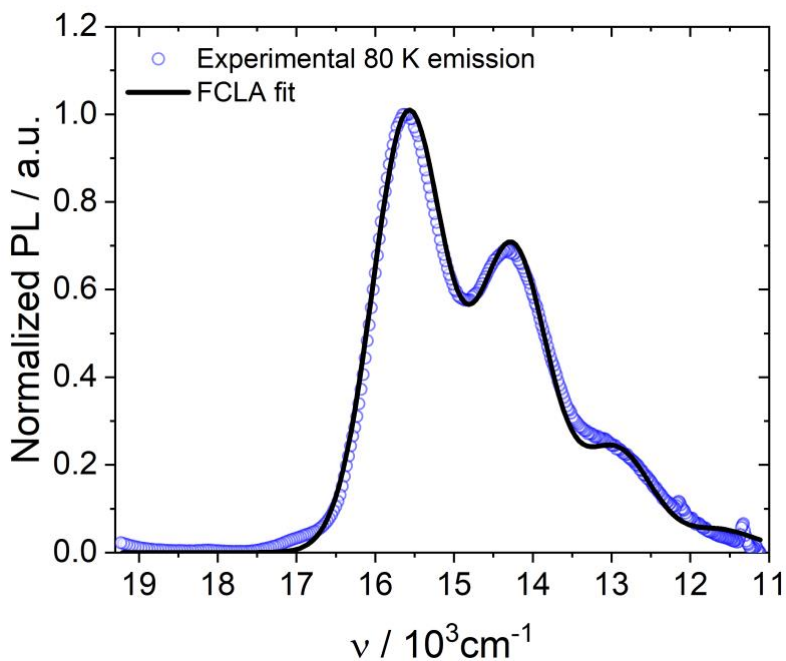


Figure S1. Franck-Condon line shape analysis of the 80 K emission of RuNCS in PN/BN under 500 nm (20000 cm^{-1}) excitation.

nsTAS and fsTAS measurements at different temperatures

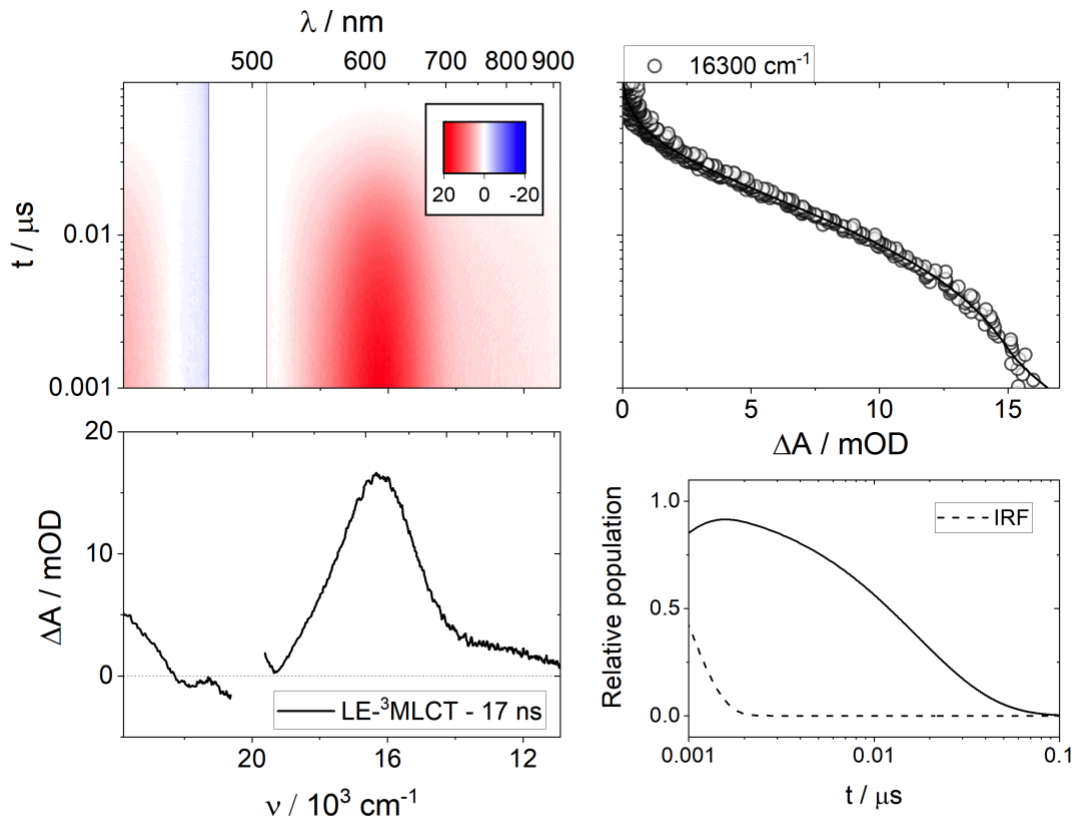


Figure S2. Differential absorption contour map obtained from nsTAS with 20000 cm^{-1} (500 nm) excitation of RuNCS in PN/BN at room temperature (upper left). Species associated differential spectra (bottom left). Differential absorption kinetic traces at 16300 cm^{-1} (upper right), and time evolution of the excited state populations (bottom right). The kinetic model involves only one excited state. IRF is the instrument response function.

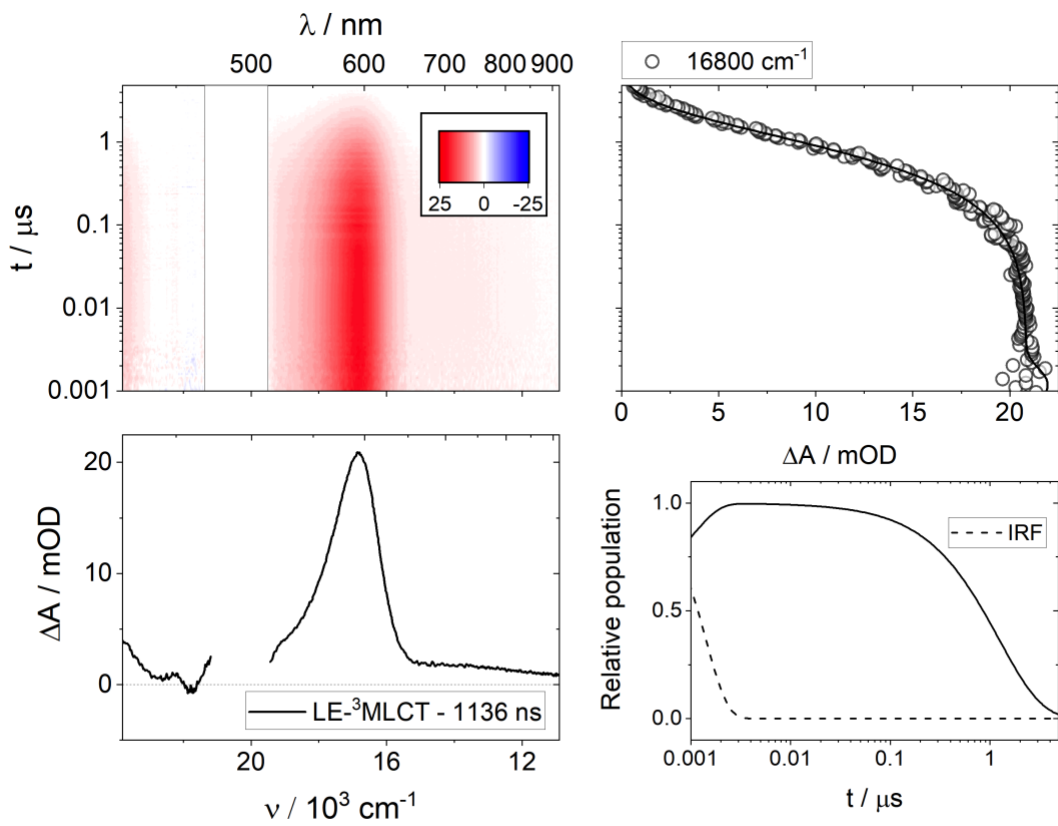


Figure S3. Differential absorption contour map obtained from nsTAS with 20000 cm^{-1} (500 nm) excitation of RuNCS in PN/BN at 80 K (upper left). Species associated differential spectra (bottom left). Differential absorption kinetic traces at 16800 cm^{-1} (upper right), and time evolution of the excited state populations (bottom right). The kinetic model involves only one excited state. IRF is the instrument response function.

T / K	nsTAS		fsTAS	
	$k_{\text{obs}} / \text{s}^{-1}$		$k_{\text{obs}} / \text{s}^{-1}$	
	ground state recovery	intermediate process	ground state recovery	intermediate process
349	$(4.375 \pm 0.007) \times 10^8$	a		
344	$(3.671 \pm 0.005) \times 10^8$	a		
340	$(3.092 \pm 0.003) \times 10^8$	a		
336	$(2.655 \pm 0.002) \times 10^8$	a		
332	$(2.285 \pm 0.002) \times 10^8$	a		
328	$(1.939 \pm 0.001) \times 10^8$	a		
324	$(1.6336 \pm 0.0008) \times 10^8$	a		
320	$(1.3773 \pm 0.0006) \times 10^8$	a		
316	$(1.1881 \pm 0.0005) \times 10^8$	a		
312	$(1.0052 \pm 0.0003) \times 10^8$	a		
308	$(8.612 \pm 0.003) \times 10^7$	a		
304	$(7.498 \pm 0.002) \times 10^7$	a		
301	$(6.693 \pm 0.002) \times 10^7$	a		
298	$(6.001 \pm 0.002) \times 10^7$	a	a	$(1.32 \pm 0.02) \times 10^{10}$
295	$(5.154 \pm 0.002) \times 10^7$	a		
290	$(4.468 \pm 0.002) \times 10^7$	a		
285	$(3.772 \pm 0.002) \times 10^7$	a		
280	$(3.196 \pm 0.001) \times 10^7$	a		
275	$(2.764 \pm 0.001) \times 10^7$	a		
270	$(2.407 \pm 0.001) \times 10^7$	a	a	$(9.1 \pm 0.1) \times 10^9$
265	$(2.165 \pm 0.001) \times 10^7$	a		
260	$(1.965 \pm 0.001) \times 10^7$	a	a	$(7.51 \pm 0.07) \times 10^9$
255	$(1.767 \pm 0.001) \times 10^7$	a		
250	$(1.676 \pm 0.001) \times 10^7$	a	a	$(5.96 \pm 0.07) \times 10^9$
245	$(1.609 \pm 0.001) \times 10^7$	a		
240	$(1.541 \pm 0.001) \times 10^7$	a	a	$(4.37 \pm 0.04) \times 10^9$
235	$(1.480 \pm 0.001) \times 10^7$	a		
230	$(1.440 \pm 0.001) \times 10^7$	a	a	$(3.57 \pm 0.04) \times 10^9$
225	$(1.389 \pm 0.001) \times 10^7$	a		
220	$(1.361 \pm 0.001) \times 10^7$	a	a	$(2.44 \pm 0.03) \times 10^9$
215	$(1.298 \pm 0.001) \times 10^7$	a		
210	$(1.277 \pm 0.001) \times 10^7$	a	a	$(1.58 \pm 0.02) \times 10^9$
205	$(1.243 \pm 0.001) \times 10^7$	a		
200	$(1.203 \pm 0.002) \times 10^7$	a	a	$(9.5 \pm 0.2) \times 10^8$
190			a	$(1.08 \pm 0.02) \times 10^9$
180	$(1.142 \pm 0.001) \times 10^7$	$(4.67 \pm 0.07) \times 10^8$	a	$(5.1 \pm 0.1) \times 10^8$
160	$(1.012 \pm 0.003) \times 10^7$	$(1.15 \pm 0.03) \times 10^8$	a	a
140	$(9.27 \pm 0.02) \times 10^6$	$(4.35 \pm 0.07) \times 10^7$	a	a
120	$(6.11 \pm 0.05) \times 10^6$	$(1.08 \pm 0.02) \times 10^7$	a	a
100	$(1.292 \pm 0.002) \times 10^6$	n.o.	a	a
80	$(8.81 \pm 0.02) \times 10^5$	n.o.	a	a

Table S1. Observed time constants extracted from global analysis of nsTAS and fsTAS experiments on RuNCS in PN/BN at different temperatures. ^a Out of experimental time-window. n.o.: not observed.

Observations

300 – 350 K: In fsTAS, the intermediate process is too fast to be determined separately from vibrational cooling components. In nsTAS, only ground state recovery is observed.

190 – 300 K: In fsTAS, an intermediate process is observed. In nsTAS, only ground state recovery is observed.

120 -190 K: In fsTAS, the intermediate process is too slow and starts escaping from experimental time-window. In nsTAS, both the intermediate process and ground state recovery are observed.

80 -120 K: In fsTAS, the intermediate process is too slow, and a mixture of HE-³MLCT and LE-³MLCT is observed. In nsTAS, only ground state recovery is observed. The lack of spectral changes that accompany the intermediate process obscures the individualization of HE-³MLCT behind the major population fraction of LE-³MLCT.

At 80K, HE-³MLCT and LE-³MLCT must have similar decays in the order of 10^6 s^{-1} , and therefore their contributions are difficult to individualize.

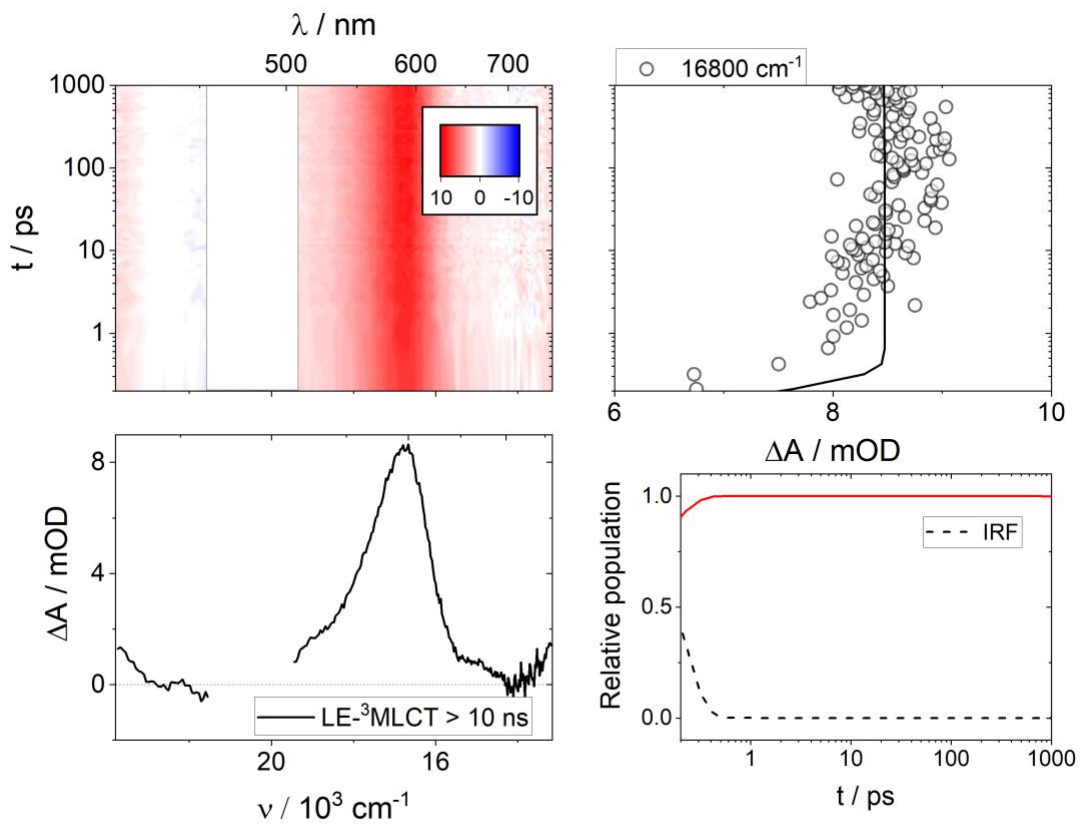


Figure S4. Differential absorption 3D map obtained from fsTAS with 20000 cm^{-1} (500 nm) excitation of RuNCS in PN/BN at 80 K (upper left). Species associated differential spectra (bottom left). Differential absorption kinetic traces at 16800 cm^{-1} (upper right), and time evolution of the excited state populations (bottom right). IRF is the instrument response function.

Theoretical Calculations

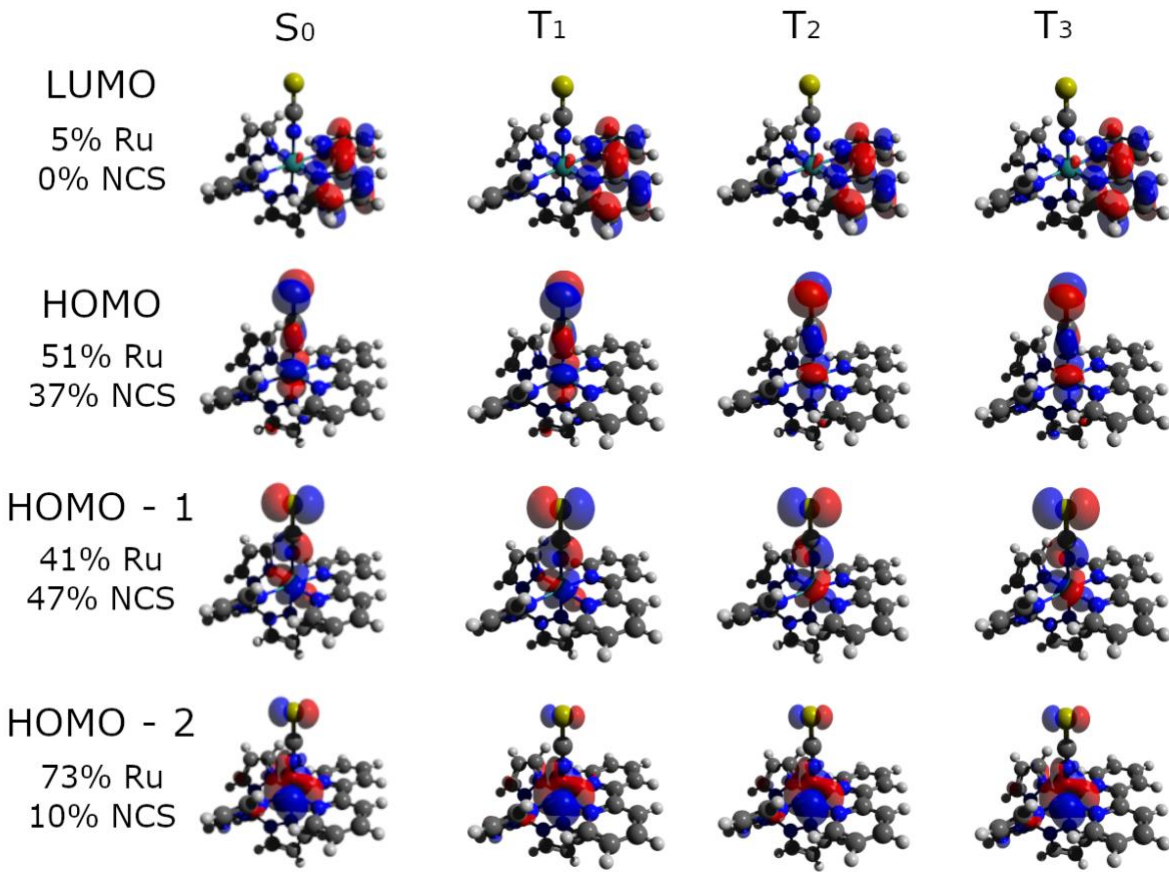


Figure S5. Frontier orbitals at the ground (S_0) and first three excited triplet state (T_{1-3}) geometries (isovalue=0.04). For each orbital, the amount of charge present on the Ruthenium atom and the NCS-ligand is given (differing less than 2% depending on the geometry).

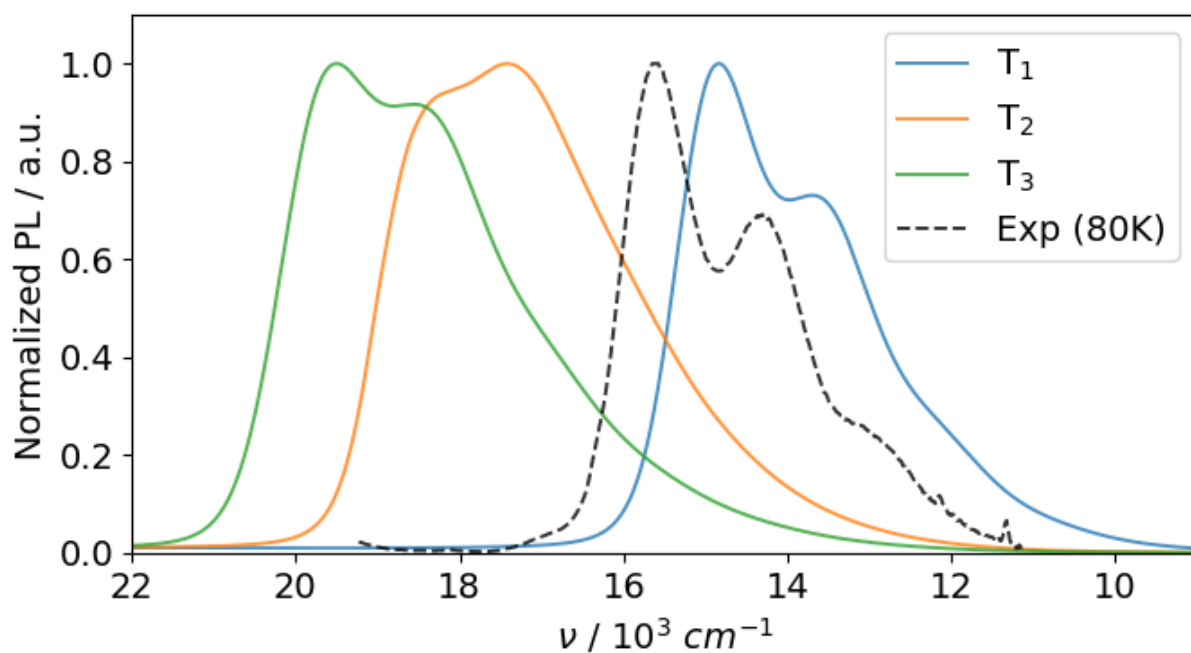


Figure S6. Calculated phosphorescence spectra of T₁₋₃., together with the experimental emission spectrum at 80K.

Transition	Energy / cm ⁻¹	Oscillator Strength	Assignment
T ₁ → T ₁₂	13318	0.23	π(NCS)→dπ(Ru) LMCT
T ₁ → T ₃₇	23900	0.35	π(bpy)→dπ(Ru) LMCT
T ₂ → T ₁₅	12473	0.16	π(NCS)→dπ(Ru) LMCT
T ₂ → T ₄₅	23758	0.34	π(bpy)→dπ(Ru) LMCT
T ₃ → T ₂₄	13435	0.07	π(bpy)→π*(bpy) IL

Table S2. Vertical transition energy, oscillator strength and assignment of the largest contributions ($f > 0.1$ except for T₃) to the calculated ESA of T₁₋₃.

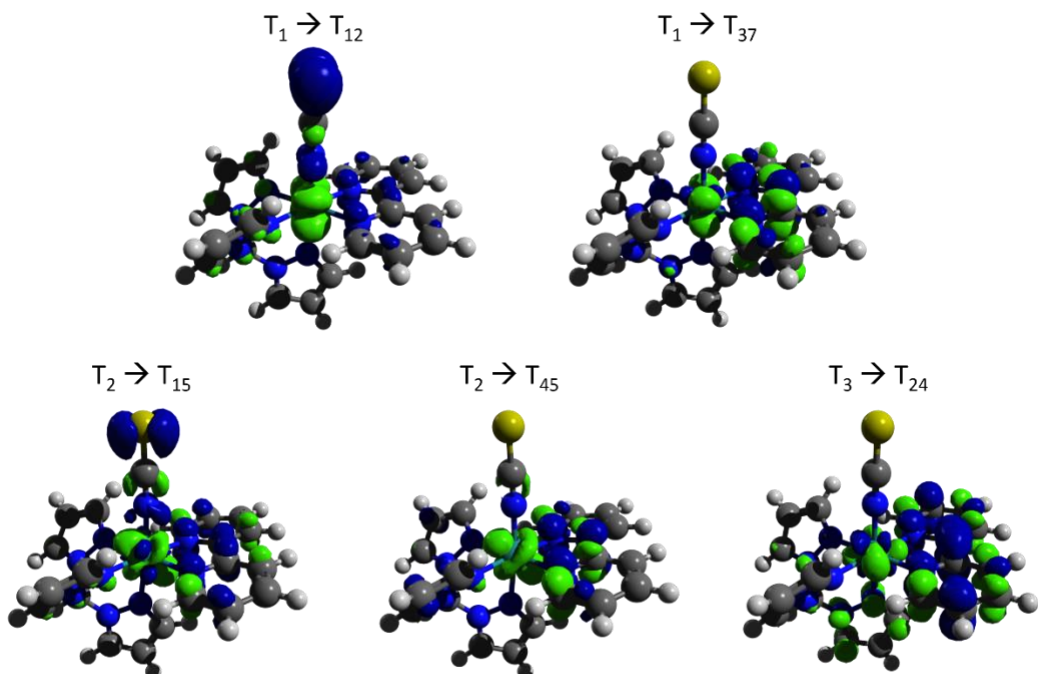


Figure S7. Electron density difference plots of the transitions listed in Table S2 (isovalue=0.002). The green color represents a bigger density in the higher state.

S₀ geometry

Ru	-0.018476	0.081140	-0.001768	H	-3.289114	1.814831	-3.901584
S	1.800767	4.602618	-0.227642	C	-2.916199	1.562372	2.910678
N	-1.512982	0.563618	-1.419959	H	-3.283308	2.136521	3.747574
N	-2.768382	0.195931	1.190697	C	3.809994	-1.149133	-1.470445
N	1.487004	-0.562195	-1.289127	H	4.766737	-1.329498	-0.996304
C	1.190737	3.073144	-0.150032	C	2.465638	-0.688718	3.516029
C	-3.045017	-0.636044	0.033517	H	2.323492	-0.674130	4.590727
H	-4.101400	-0.893738	0.047719	C	1.386813	-0.433164	2.676619
N	-1.510771	0.690891	1.370922	H	0.402799	-0.218451	3.073785
N	-0.917887	-1.808860	0.085414	C	-1.605417	-3.959214	0.167822
N	-2.279763	-1.865216	0.082608	H	-1.580483	-5.037325	0.210585
C	-2.723740	-3.153756	0.131454	C	3.825410	-0.972920	1.559439
H	-3.779225	-3.382454	0.135242	H	4.781590	-1.189238	1.099402
N	-2.773241	0.097118	-1.189995	C	1.367961	-0.704520	-2.621794
C	2.700834	-0.720044	0.768695	H	0.382713	-0.523272	-3.032458
N	1.495104	-0.431240	1.335556	C	3.684316	-1.274591	-2.850931
C	-3.647412	0.540979	-2.137891	H	4.544128	-1.544461	-3.454969
H	-4.692587	0.270978	-2.105640	C	-0.505676	-3.078005	0.137373
N	0.751825	1.981385	-0.094638	H	0.551145	-3.300866	0.149713
C	-1.599632	1.301387	-2.528992	C	-1.597779	1.520984	2.412701
H	-0.718787	1.791985	-2.916937	H	-0.719390	2.050898	2.751492
C	-3.640938	0.711973	2.102861	C	3.710940	-0.951313	2.946444
H	-4.683679	0.430167	2.101372	H	4.578377	-1.144252	3.568775
C	2.694976	-0.799423	-0.703411	C	2.437538	-1.058902	-3.436741
C	-2.920949	1.311800	-3.020546				

Table S3. XYZ coordinates in Angstrom of the optimized S₀ state.

T₁ geometry

Ru	-0.004124	0.133445	-0.000252	H	-3.421878	1.853263	-3.809773
S	1.686358	4.613504	-0.012020	C	-3.017425	1.341787	2.951907
N	-1.559830	0.596839	-1.398629	H	-3.421511	1.865952	3.804231
N	-2.783887	0.040694	1.190300	C	3.822998	-1.037595	-1.531410
N	1.478954	-0.433482	-1.315314	H	4.779442	-1.253610	-1.068977
C	1.105839	3.097432	-0.007636	C	2.433353	-0.772081	3.495032
C	-3.006545	-0.761782	0.001551	H	2.290639	-0.793942	4.568903
H	-4.041635	-1.094615	0.002056	C	1.375722	-0.467431	2.665238
N	-1.560040	0.602808	1.396132	H	0.394470	-0.246188	3.068477
N	-0.800772	-1.796641	0.004064	C	-1.334759	-3.984985	0.008538
N	-2.157354	-1.939732	0.003875	H	-1.241100	-5.059916	0.010893
C	-2.507609	-3.251767	0.006594	C	3.824137	-1.027112	1.535916
H	-3.543957	-3.556627	0.006989	H	4.780736	-1.244147	1.074287
N	-2.783954	0.036373	-1.190076	C	1.374607	-0.481953	-2.662822
C	2.702702	-0.730095	0.711010	H	0.393308	-0.262319	-3.066827
N	1.479326	-0.426763	1.317420	C	3.695809	-1.066058	-2.898624
C	-3.688127	0.471077	-2.112010	H	4.553059	-1.301025	-3.521685
H	-4.713647	0.132834	-2.094000	C	-0.299750	-3.037058	0.006819
N	0.675504	1.993988	-0.004724	H	0.770495	-3.182868	0.007418
C	-1.697021	1.381382	-2.469455	C	-1.697182	1.390893	2.464369
H	-0.851290	1.944429	-2.836975	H	-0.851662	1.955875	2.829392
C	-3.687718	0.477506	2.111562	C	3.697648	-1.047733	2.903335
H	-4.712901	0.138092	2.095574	H	4.555529	-1.277798	3.527355
C	2.702350	-0.734311	-0.707711	C	2.431557	-0.792377	-3.491332
C	-3.017641	1.331714	-2.955917				

Table S4. XYZ coordinates in Angstrom of the optimized T₁ state.

T₂ geometry

Ru	-0.012557	0.114219	-0.000129	H	3.326747	1.817964	3.864484
S	-1.407720	4.681044	-0.005632	C	2.940844	1.297462	-3.000392
N	1.511245	0.558168	1.419973	H	3.326934	1.809205	-3.868412
N	2.758321	0.051465	-1.192789	C	-3.880938	-0.899654	1.536356
N	-1.506491	-0.460794	1.316354	H	-4.854003	-1.034418	1.077252
C	-0.960892	3.122077	-0.003819	C	-2.464103	-0.814576	-3.491197
C	3.006886	-0.738567	0.000931	H	-2.315535	-0.886025	-4.562141
H	4.052984	-1.034770	0.001330	C	-1.394432	-0.561535	-2.661855
N	1.511288	0.554703	-1.421292	H	-0.395957	-0.427112	-3.060898
N	0.840011	-1.829639	0.002275	C	1.428308	-4.003326	0.004880
N	2.195433	-1.938955	0.002286	H	1.356860	-5.080028	0.006187
C	2.581029	-3.246207	0.003854	C	-3.880639	-0.904178	-1.534493
H	3.625461	-3.520845	0.004077	H	-4.853695	-1.038194	-1.075151
N	2.758244	0.054244	1.192782	C	-1.394776	-0.554768	2.663143
C	-2.747856	-0.672591	-0.711397	H	-0.396320	-0.419556	3.061967
N	-1.506359	-0.464015	-1.315336	C	-3.749389	-0.964151	2.904518
C	3.642784	0.492464	2.129461	H	-4.619631	-1.144535	3.527762
H	4.680359	0.193684	2.103199	C	0.367348	-3.076396	0.003840
N	-0.641428	1.981140	-0.002433	H	-0.699201	-3.247512	0.004132
C	1.620501	1.318925	2.512358	C	1.620563	1.312940	-2.515426
H	0.754732	1.841067	2.893055	H	0.754757	1.834037	-2.897463
C	3.642923	0.487713	-2.130328	C	-3.748885	-0.972272	-2.902460
H	4.680536	0.189161	-2.103238	H	-4.618971	-1.154681	-3.525333
C	-2.747961	-0.670674	0.712800	C	-2.464629	-0.805329	3.493005
C	2.940706	1.304309	2.997572	H	-2.316223	-0.874017	4.564151

Table S5. XYZ coordinates in Angstrom of the optimized T₂ state.

T₃ geometry

Ru	0.019403	0.140103	0.014824	H	3.513305	1.660372	3.793942
S	-1.641467	4.690249	0.261200	C	3.059919	1.517373	-2.787582
N	1.579700	0.498625	1.396058	H	3.488846	2.113927	-3.577737
N	2.763544	0.015155	-1.198273	C	-3.792954	-1.187431	1.477717
N	-1.482518	-0.484213	1.302843	H	-4.737666	-1.421950	1.000483
C	-1.068548	3.158212	0.192524	C	-2.462257	-0.461608	-3.524825
C	2.971022	-0.871888	-0.059560	H	-2.333528	-0.370864	-4.596753
H	3.998418	-1.226043	-0.083627	C	-1.405198	-0.199007	-2.680653
N	1.573884	0.676624	-1.317890	H	-0.439067	0.098140	-3.071490
N	0.745111	-1.826796	-0.119770	C	1.203225	-4.026201	-0.273296
N	2.092540	-2.017598	-0.131014	H	1.067564	-5.094102	-0.347847
C	2.399603	-3.341900	-0.224254	C	-3.810431	-0.960215	-1.584435
H	3.425212	-3.679728	-0.247408	H	-4.752242	-1.254843	-1.135649
N	2.771149	-0.135450	1.182734	C	-1.379576	-0.577316	2.648183
C	-2.694489	-0.692526	-0.744678	H	-0.410408	-0.333738	3.067656
N	-1.493071	-0.302586	-1.335040	C	-3.670461	-1.273522	2.843574
C	3.700368	0.269318	2.091557	H	-4.519289	-1.575640	3.448851
H	4.712595	-0.106125	2.061905	C	0.199784	-3.039797	-0.205126
N	-0.655880	2.054945	0.147316	H	-0.874997	-3.147480	-0.213701
C	1.763653	1.286589	2.459833	C	1.751862	1.588895	-2.278389
H	0.948815	1.894067	2.826083	H	0.937038	2.241128	-2.557453
C	3.685056	0.521975	-2.062555	C	-3.702466	-0.848203	-2.949612
H	4.693969	0.137051	-2.092947	H	-4.559633	-1.054275	-3.582825
C	-2.687698	-0.793847	0.674258	C	-2.426006	-0.966313	3.456068
C	3.078212	1.162609	2.941219	H	-2.286113	-1.030542	4.528517

Table S6. XYZ coordinates in Angstrom of the optimized T₃ state.

MECI geometry

Ru	3.3491619219	2.0909863700	10.2888595302	H	7.6903387112	4.5900404225	8.2160763211
S	5.6096545091	-2.0414196748	8.7818561125	C	5.6266601791	1.9276254704	14.0312714386
N	5.0383728419	3.2932615841	9.6873266945	H	6.0943712958	1.4639271995	14.8832426019
N	4.8740920725	3.4172350203	12.5759524707	C	0.1114807584	2.1672602646	7.4383963470
N	2.2771619473	2.4216439798	8.5203311114	H	-0.8993266637	1.7779424434	7.4567507409
C	4.8664862573	-0.6110968328	9.3092662561	C	0.3327395899	-0.4661307348	11.9697778313
C	4.6573863088	4.5960483605	11.7425799770	H	0.2487916374	-1.1269693752	12.8231466815
H	5.0903886044	5.4605604151	12.2382511188	C	1.5491622831	0.0985170902	11.6511047593
N	4.4705848621	2.1824456893	12.1091803079	H	2.4416945528	-0.0858878569	12.2365507090
N	2.4332482389	3.8500790112	10.9964380162	C	1.1730652014	5.6301128150	11.5941470718
N	3.2350641216	4.8255142015	11.5648141690	H	0.3170828884	6.2667609017	11.7408890922
C	2.4872495375	5.9089924904	11.9372724717	C	-0.6524943140	0.6367541933	10.0355815229
H	2.9435342412	6.7653022319	12.4055043868	H	-1.5004726195	0.8470862528	9.3944919619
N	5.3297916502	4.4061239509	10.4601059842	C	2.7277347452	3.0723202385	7.4117270907
C	0.6131981436	1.1937269931	9.7185600079	H	3.7512062960	3.4154600456	7.4396115009
N	1.6896746276	0.9498911330	10.5881971699	C	0.5795020856	2.8520983977	6.3324682149
C	6.4416054536	5.0467758038	9.9782093300	H	-0.0691730101	3.0215913629	5.4805262306
H	6.8375961086	5.9182985145	10.4726724705	C	1.1815104192	4.3416080821	11.0133882683
N	4.3522469777	0.3891588152	9.6777886392	H	0.3656501139	3.7642323639	10.6135994663
C	5.9650372293	3.2618167194	8.7134327234	C	4.9291780319	1.2739158964	12.9888691564
H	5.9474348330	2.4845807120	7.9676322674	H	4.7362030270	0.2243851781	12.8436553070
C	5.5895117437	3.2820539999	13.7353544087	C	-0.7980872272	-0.1749114808	11.1460861988
H	6.0038076327	4.1405434270	14.2371393093	H	-1.7644521998	-0.6056224262	11.3822467360
C	0.9584016936	1.9359098475	8.5540216316	C	1.9233052367	3.3128103469	6.3119304828
C	6.8558827200	4.3514216427	8.8534777026	H	2.3224477031	3.8486165027	5.4601330005

Table S7. XYZ coordinates in Angstrom of the optimized MECI state.

Contributions to the observed decay constants for LE- 3 MLCT and HE- 3 MLCT

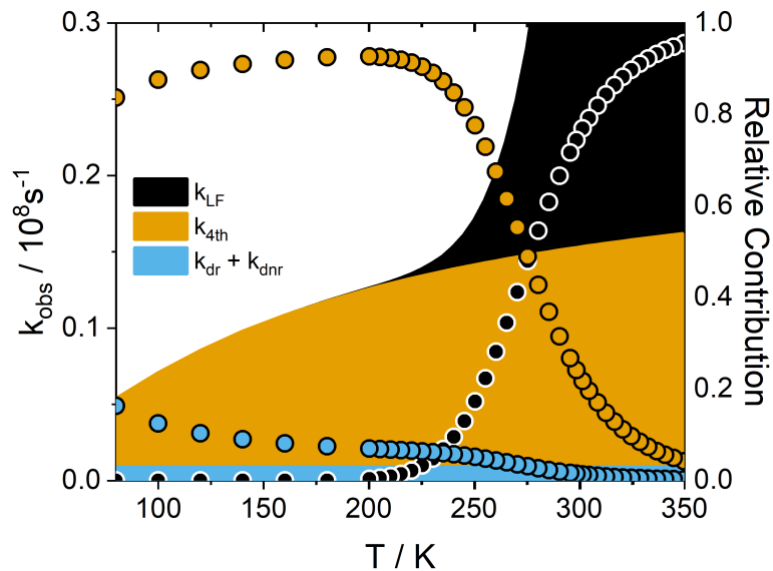


Figure S8. Additive (areas, left axis) and relative (dots, right axis) contributions to the observed decay constant of LE- 3 MLCT as a function of temperature.

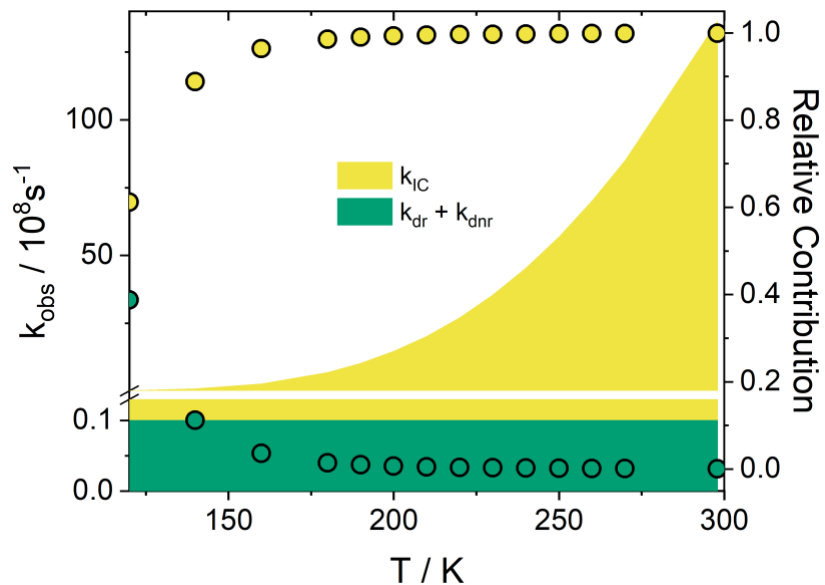


Figure S9. Additive (areas, left axis) and relative (dots, right axis) contributions to the observed decay constant of HE- 3 MLCT as a function of temperature.

Density descriptors for excited state interconversions

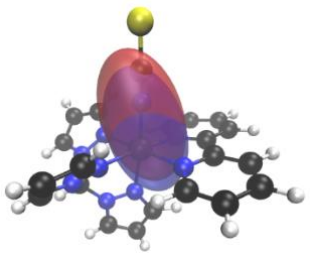
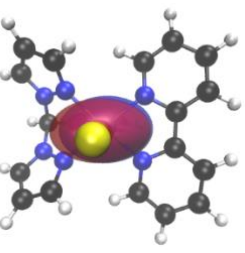
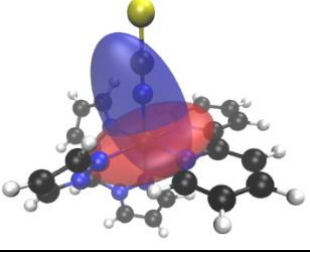
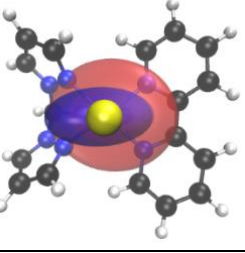
Transition	D (Å)	S \pm	Side view	Top view
T2 → T1	0.6	0.98		
T3 → T2	1.2	0.60		

Figure S10. Dependence Computed values of the the S \pm and D (Å) indexes for the T₃ → T₂ and T₂ → T₁ IC processes. A visual representation of the C₊ and C₋ functions is also shown. See definitions of functions and descriptors in Ref. [27].

Solvent dependence of IC rates

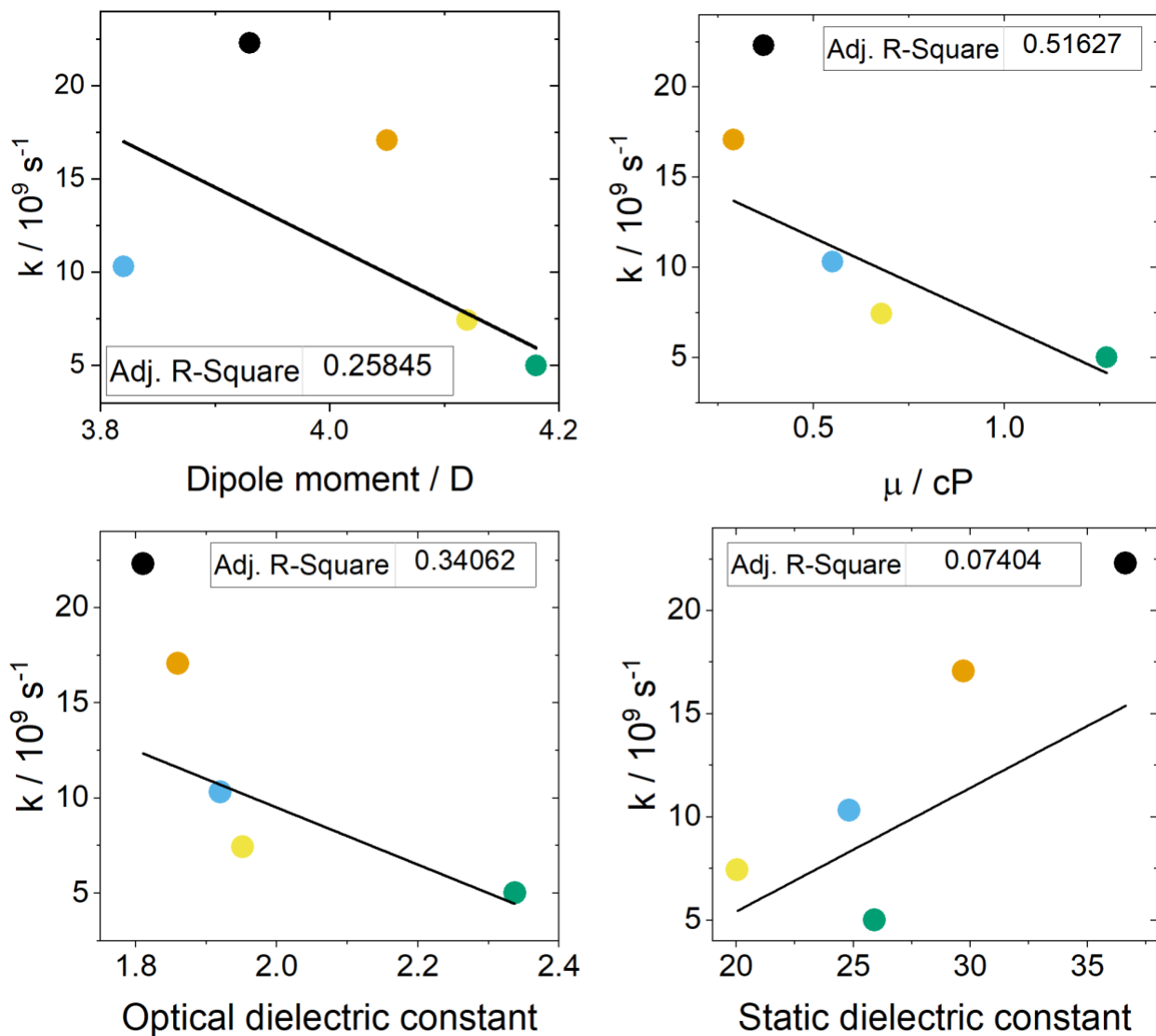


Figure S11. Dependence of HE-³MLCT decay constants on the dipole moment (top left), viscosity (top right), optical dielectric constant (bottom left), and the static dielectric constant (bottom right), in acetonitrile (black), propionitrile (orange), butyronitrile (cyan), valeronitrile (yellow) and benzonitrile (green) at 298 K.

References

- [1] A. Cadranel, P. S. Oviedo, G. E. Pieslinger, S. Yamazaki, V. D. Kleiman, L. M. Baraldo and D. M. Guldi, *Chem. Sci.*, 2017, **8**, 7434–7442.
- [2] K. Suzuki, A. Kobayashi, S. Kaneko, K. Takehira, T. Yoshihara, H. Ishida, Y. Shiina, S. Oishi and S. Tobita, *Phys. Chem. Chem. Phys.*, 2009, **11**, 9850–9860.
- [3] I. H. M. Van Stokkum, D. S. Larsen and R. Van Grondelle, *Biochim. Biophys. Acta - Bioenerg.*, 2004, **1657**, 82–104.
- [4] J. J. Snellenburg, S. Laptenok, R. Seger, K. M. Mullen and I. H. M. van Stokkum, *J. Stat. Softw.*, 2012, **49**, 1–22.
- [5] K. M. Mullen and I. H. M. Van Stokkum, *J. Stat. Softw.*, 2007, **18**, 1–46.
- [6] W. R. Roberts, T. N. Rohrbaugh and R. M. O'Donnell, *J. Vis. Exp.*, 2021, 1–13.
- [7] P. Hohenberg and W. Kohn, *Phys. Rev.*, 1964, **136**, B864–B871.
- [8] W. Kohn and L. J. Sham, *Phys. Rev.*, 1965, **140**, A1133–A1138.
- [9] D. R. SALAHUB and M. C. ZERNER, *The Challenge of d and f Electrons*, American Chemical Society, Washington, DC, 1989, vol. 394.
- [10] R. G. Parr and Y. Weitao, *Density-Functional Theory of Atoms and Molecules*, Oxford University Press, 1995.
- [11] E. Runge and E. K. U. Gross, *Phys. Rev. Lett.*, 1984, **52**, 997–1000.
- [12] M. E. Casida, *J. Mol. Struct. THEOCHEM*, 2009, **914**, 3–18.
- [13] A. D. Becke, *J. Chem. Phys.*, 1993, **98**, 5648–5652.
- [14] W. J. Hehre, R. Ditchfield and J. A. Pople, *J. Chem. Phys.*, 1972, **56**, 2257–2261.
- [15] D. Andrae, U. Haeussermann, M. Dolg, H. Stoll and H. Preuss, *Theor. Chim. Acta*, 1990, **77**, 123–141.
- [16] J. Tomasi, B. Mennucci and R. Cammi, *Chem. Rev.*, 2005, **105**, 2999–3094.
- [17] M. J. Frisch, G. W. Trucks, H. B. Schlegel, G. E. Scuseria, M. A. Robb, J. R. Cheeseman, G. Scalmani, V. Barone, G. A. Petersson, H. Nakatsuji, X. Li, M. Caricato, A. V. Marenich, J. Bloino, B. G. Janesko, R. Gomperts, B. Mennucci, H. P. Hratchian, J. V. Ortiz, A. F. Izmaylov, J. L. Sonnenberg, D. Williams-Young, F. Ding, F. Lipparini, F. Egidi, J. Goings, B. Peng, A. Petrone, T. Henderson, D. Ranasinghe, V. G. Zakrzewski, J. Gao, N. Rega, G. Zheng, W. Liang, M. Hada, M. Ehara, K. Toyota, R. Fukuda, J. Hasegawa, M. Ishida, T. Nakajima, Y. Honda, O. Kitao, H. Nakai, T. Vreven, K. Throssell, J. A. Montgomery Jr., J. E. Peralta, F. Ogliaro, M. J. Bearpark, J. J. Heyd, E. N. Brothers, K. N. Kudin, V. N. Staroverov, T. A. Keith, R. Kobayashi, J. Normand, K. Raghavachari, A. P. Rendell, J. C. Burant, S. S. Iyengar, J. Tomasi, M. Cossi, J. M. Millam, M. Klene, C. Adamo, R. Cammi, J. W. Ochterski, R. L. Martin, K. Morokuma, O. Farkas, J. B. Foresman and D. J. Fox, Gaussian Inc., Wallingford CT, 2016.
- [18] Z. Liu, T. Lu and Q. Chen, *Carbon N. Y.*, 2020, **165**, 461–467.
- [19] T. Lu and F. Chen, *Acta Chim. Sin.*, 2011, **69**, 2393–2406.
- [20] B. de Souza, G. Farias, F. Neese and R. Izsák, *J. Chem. Theory Comput.*, 2019, **15**, 1896–1904.
- [21] E. van Lenthe, J. G. Snijders and E. J. Baerends, *J. Chem. Phys.*, 1996, **105**, 6505–6516.
- [22] F. Weigend and R. Ahlrichs, *Phys. Chem. Chem. Phys.*, 2005, **7**, 3297.
- [23] V. Barone and M. Cossi, *J. Phys. Chem. A*, 1998, **102**, 1995–2001.
- [24] B. Helmich-Paris, B. de Souza, F. Neese and R. Izsák, *J. Chem. Phys.*, 2021, **155**, 104109.
- [25] Y. Shao, M. Head-Gordon and A. I. Krylov, *J. Chem. Phys.*, 2003, **118**, 4807–4818.

- [26] Y. Shao, Z. Gan, E. Epifanovsky, A. T. B. Gilbert, M. Wormit, J. Kussmann, A. W. Lange, A. Behn, J. Deng, X. Feng, D. Ghosh, M. Goldey, P. R. Horn, L. D. Jacobson, I. Kaliman, R. Z. Khaliullin, T. Kuś, A. Landau, J. Liu, E. I. Proynov, Y. M. Rhee, R. M. Richard, M. A. Rohrdanz, R. P. Steele, E. J. Sundstrom, H. L. Woodcock, P. M. Zimmerman, D. Zuev, B. Albrecht, E. Alguire, B. Austin, G. J. O. Beran, Y. A. Bernard, E. Berquist, K. Brandhorst, K. B. Bravaya, S. T. Brown, D. Casanova, C.-M. Chang, Y. Chen, S. H. Chien, K. D. Closser, D. L. Crittenden, M. Diedenhofen, R. A. DiStasio, H. Do, A. D. Dutoi, R. G. Edgar, S. Fatehi, L. Fusti-Molnar, A. Ghysels, A. Golubeva-Zadorozhnaya, J. Gomes, M. W. D. Hanson-Heine, P. H. P. Harbach, A. W. Hauser, E. G. Hohenstein, Z. C. Holden, T.-C. Jagau, H. Ji, B. Kaduk, K. Khistyayev, J. Kim, J. Kim, R. A. King, P. Klunzinger, D. Kosenkov, T. Kowalczyk, C. M. Krauter, K. U. Lao, A. D. Laurent, K. V. Lawler, S. V. Levchenko, C. Y. Lin, F. Liu, E. Livshits, R. C. Lochan, A. Luenser, P. Manohar, S. F. Manzer, S.-P. Mao, N. Mardirossian, A. V. Marenich, S. A. Maurer, N. J. Mayhall, E. Neuscamman, C. M. Oana, R. Olivares-Amaya, D. P. O'Neill, J. A. Parkhill, T. M. Perrine, R. Peverati, A. Prociuk, D. R. Rehn, E. Rosta, N. J. Russ, S. M. Sharada, S. Sharma, D. W. Small, A. Sodt, T. Stein, D. Stück, Y.-C. Su, A. J. W. Thom, T. Tsuchimochi, V. Vanovschi, L. Vogt, O. Vydrov, T. Wang, M. A. Watson, J. Wenzel, A. White, C. F. Williams, J. Yang, S. Yeganeh, S. R. Yost, Z.-Q. You, I. Y. Zhang, X. Zhang, Y. Zhao, B. R. Brooks, G. K. L. Chan, D. M. Chipman, C. J. Cramer, W. A. Goddard, M. S. Gordon, W. J. Hehre, A. Klamt, H. F. Schaefer, M. W. Schmidt, C. D. Sherrill, D. G. Truhlar, A. Warshel, X. Xu, A. Aspuru-Guzik, R. Baer, A. T. Bell, N. A. Besley, J.-D. Chai, A. Dreuw, B. D. Dunietz, T. R. Furlani, S. R. Gwaltney, C.-P. Hsu, Y. Jung, J. Kong, D. S. Lambrecht, W. Liang, C. Ochsenfeld, V. A. Rassolov, L. V. Slipchenko, J. E. Subotnik, T. Van Voorhis, J. M. Herbert, A. I. Krylov, P. M. W. Gill and M. Head-Gordon, *Mol. Phys.*, 2015, **113**, 184–215.
- [27] K. Veys and D. Escudero, *Acc. Chem. Res.*, DOI:10.1021/acs.accounts.2c00453.